CCFE
CULHAM CENTRE FOR FUSION ENERGY

UK Atomic Energy Authority

UKAEA-CCFE-PR(25)397

Andrew Bulla, Andrew J. London, Christina Hofer,
Paul A.J. Bagot, Michael P. Moody

Atom Probe Tomography investigation of lithium uptake from liquid Pb- 17Li by nanocrystalline/amorphous Al2O3 coatings

Atom Probe Tomography investigation of lithium uptake from liquid Pb- 17Li by nanocrystalline/amorphous Al2O3 coatings

Andrew Bulla, Andrew J. London, Christina Hofer, Paul A.J. Bagot, Michael P. Moody

This is a preprint of a paper submitted for publication in Corrosion Science

Corrosion Science 238 (2024) 112363

Contents lists available at ScienceDirect

Corrosion Science

journal homepage: www.elsevier.com/locate/corsci

Atom Probe Tomography investigation of lithium uptake from liquid Pb-17Li by nanocrystalline/amorphous Al_2O_3 coatings

Andrew Bulla [a,*], Andrew J. London [b], Christina Hofer [a], Paul A.J. Bagot [a], Michael P. Moody [a]

[a] Department of Materials, University of Oxford, Parks Road, Oxford OX1 3PH, United Kingdom
[b] UK Atomic Energy Authority, Culham Campus, Abingdon OX14 3DB, United Kingdom

ARTICLE INFO

Keywords:
Liquid metal
Alumina
Atom probe tomography
Amorphous material
Lithium corrosion

ABSTRACT

Atom probe tomography has been applied to study lithium-induced corrosion of Pulsed-Laser Deposition grown Al_2O_3, which is a candidate coating material for breeder blankets for nuclear fusion reactors. Coated Eurofer97 specimens were immersed in static Pb-17Li for 7000 h with samples extracted from the regions near the ceramic-substrate interface to determine the extent of Li penetration. Li-enriched regions, which are non-stoichiometric with respect to any known equilibrium phases predicted by the Li-Al-O phase diagram at 823 K, are reported for the first time in Al_2O_3. The nature and composition of the Li-enriched features were characterized with nanometre resolution. It was found that the Li content inside these features may increase to a maximum of 35 at%, with the adjacent Al_2O_3 matrix containing approximately 5–10 at% Li. Based on these results, the corrosion mechanism of amorphous Al_2O_3 is proposed to be Li substitution of Al atoms.

1. Introduction

Liquid lithium-lead eutectic (Pb-17Li) is a fundamental breeder material in several blanket design concepts for the European DEMO fusion reactor [1]. Its main role is to produce tritium fuel in-situ through neutron reaction with lithium isotopes. This fuel is then extracted and used to sustain the deuterium-tritium fusion reaction. Since pure Li would react explosively if accidentally exposed to steam from the heat extraction system, Pb is added to stabilize the highly reactive liquid Li as a neutron multiplier through the Pb(n,2 n) reaction [2]. Despite having a lower Li concentration for breeding tritium, liquid Pb-17Li preserves the excellent thermal conductivity and the immunity to radiation damage of pure Li [2]. The reduced-activation ferritic/martensitic (RAFM) steel Eurofer97 has been proposed as a candidate structural material for the blanket itself [3]. However, direct contact between Eurofer97 and Pb-17Li unavoidably entails corrosion damage to the steel.

The detailed corrosion sequence and mechanism of RAFM steels exposed to Pb-17Li have been thoroughly explored in several previous studies [4,5]. Heat treating RAFM steels forms a passivating oxide consisting of $MnCr_2O_4$ on top of $(Fe,Cr)_2O_3$[4]. Initial corrosion rates are inhomogeneous across the surface due to varying oxide composition and thickness. Pb-17Li is able to completely dissolve the less stable spinel while leaving a thin layer consisting of several nanometres of $(Fe,Cr)_2O_3$ intact after 6000 h [5]. After 3000 h of exposure to Pb-17Li, uniform corrosion proceeds through dissolution of alloying elements without intermetallic formation [4]. Fe and Cr are preferentially leached out of the matrix, which leaves behind a porous layer enriched in less soluble elements including W and V [4,6,7]. This process may eventually lead to thinning and even perforation of components such as cooling tubes embedded within the blanket. This is a serious safety concern as it has potential to facilitate explosive reactions between the Li-containing breeder and the water coolant.

In the past decade, barrier coatings such as pulsed-laser deposited (PLD) Al_2O_3, were explored to mitigate corrosion damage and prevent tritium permeation through the blanket [8]. Al_2O_3 was originally proposed as the reference tritium permeation barrier by the European Union [9], but later its anti-corrosion properties led to its adoption as a candidate barrier coating material. PLD is a physical vapour deposition technique that utilizes a laser plume to evaporate the target. The resulting coating possesses an amorphous matrix with uniform dispersion of nanocrystals ranging between 2 and 5 nm [10]. Random alignments of these crystals have led to mechanical isotropy with metal-like stiffness and no indication of delamination after scratch tests [10]. In separate studies [6–8,11], it is also proposed to be able to fully prevent liquid Pb and Pb-17Li from corrosively attacking steel substrates at temperatures up to 823 K based on energy-dispersive X-ray spectroscopy

* Corresponding author.
E-mail address: andrew.bulla@materials.ox.ac.uk (A. Bulla).

https://doi.org/10.1016/j.corsci.2024.112363
Received 8 April 2024; Received in revised form 13 June 2024; Accepted 9 August 2024
Available online 10 August 2024

(EDX) and secondary ion mass spectroscopy (SIMS) data, respectively.

However, while corrosion resistance is provided by the barrier coating, studies have demonstrated that lithium penetration through the coating is possible [6]. If unaccounted for, the accumulation of lithium at the coating-metal interface may lead to phase changes like those seen in Y_2O_3, namely the conversion of Y_2O_3 into $LiYO_2$, and subsequent coating delamination in service due to the associated volumetric expansion [12]. Understanding the effect of lithium uptake on the microstructure near the interface is therefore imperative for ensuring an extended service life for breeder blanket components.

Compared to other candidate materials, such as Er_2O_3 and Y_2O_3[12–14], Li corrosion of Al_2O_3 remains largely unexplored, and in particular there is no published literature examining the mechanism by which the Li is incorporated into the ceramic matrix in detail. Hence, its effect on the resulting near-interface microstructure remains an open question. Characterization of the thin, complex interface requires techniques with nanometre spatial resolution and extremely high chemical sensitivity. Atom probe tomography (APT) not only satisfies the above requirements, but also has the ability to reliably detect lithium atoms, something which is challenging for many electron microscopy techniques.

In this study, APT has been used to study the spatial distribution of Li in the PLD-Al_2O_3 ceramic near the Al_2O_3–Eurofer97 interface in samples exposed to static Pb-17Li for 7000 h.

2. Materials

Eurofer97 samples in the form of cylinders were made at the Italian National Agency for New Technologies, Energy and Sustainable Economic Development (ENEA). The steel has gone through the standard heat treatment described in [15] and has a nominal composition shown in Table 1. Surface treatments, including polishing and argon plasma cleaning, were performed before the application of the Al_2O_3 coating using the PLD technique. Details on the PLD parameters and setup can be found in [16]. The coating thickness was determined to be 3μm by scanning electron microscopy (SEM). Fig. 1. shows a SEM image of the cross-section near the ceramic-steel interface with the region of interest and intended position of the APT samples highlighted. No signs of interfacial delamination or micro-cracks were observed, suggesting the coating was fully dense.

The rod-shaped samples were immersed in static Pb-17Li for 7000 h at the ENEA Brasimone Research Centre. A test temperature of 823 K was chosen to simulate service conditions of ITER first walls. Oxygen content and contamination of the liquid metal were kept at a minimum.

The cross-sectioned sample surface was ground with 40μm and 9μm diamond discs, followed by 3μm gold and 1μm alumina discs. The final polishing was done with 0.05μm VelTex paper and 0.05μm colloidal alumina/silica.

2.1. Atom Probe Tomography

Atom probe tomography measurements were performed using the CAMECA Local Electrode Atom Probe (LEAP 5000 XR) with a 52 % detector efficiency. The instrument is equipped with a 355 nm UV laser and a reflectron that enhances mass resolution. The samples were run at a laser pulse energy between 40 and 50pJ, a base temperature of 50 K, a pulse frequency of 200 kHz and a detection rate (ions detected per laser pulse) of 0.5 %.

Spatial reconstruction of 3D-atom maps was conducted with the software APSuite v.6.3.1, using the standard algorithm based upon the evolution of the applied voltage profile. Regions-of-interest (ROIs) were isolated using a user-defined cylindrical volume. The mass spectra and composition measured within these ROIs were then examined to reveal any local compositional variations when compared to the bulk ceramic.

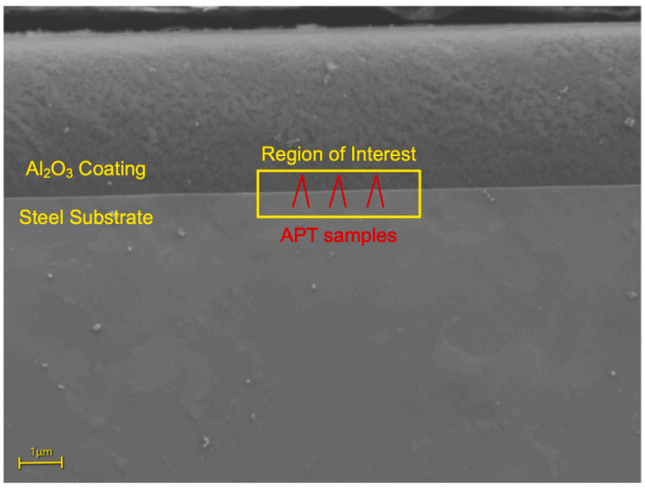

Fig. 1. Secondary electron SEM micrograph of Al_2O_3-coated Eurofer97, the yellow box highlights the sample extraction region near the ceramic-metal interface, the red needles within indicate the orientation of the APT samples with respect to the ceramic-steel interface.

2.2. APT sample preparation

A Helios NanoLab 600i dual-beam SEM/Focused Ion Beam (FIB) system was used for the preparation of APT samples from the coating-metal interface. The specimen preparation in this work was based on the standard FIB lift-out as described in Thompson et al.[18] However, a Pt layer was not applied as the Al_2O_3 was sufficiently thick to protect the interface from ion damage. Detailed stages of the lift-out and milling process are shown in Fig. 2. The lamella was attached to a sample holder containing Si flat top posts. The final annular milling step was conducted with decreasing inner radius from 2.5μm to 120 nm, starting with an ion accelerating voltage of 30 kV (9.3 nA current), decreasing to a final 2 kV (190pA current) cleaning step to minimise beam damage and to reach $<$100 nm from the Al_2O_3-steel interface.

A bright halo was observed near the ceramic-steel interface in Fig. 3., obtained by the Helios SEM/FIB in-lens detector during annular milling for APT sample preparation. The nature of this interface layer remains unclear, given that similar structures were not previously reported. It is speculated that the brightness could come from electron charging effects arising from the sudden change in electrical conductivity near the interface. However, there is no clear evidence that the two phenomena are directly related and thus no definitive conclusions can be drawn from within the scope of this study.

2.3. Complementary microscopy

Complementary micro-scale characterization was performed on metallographic samples. EDX and SEM imaging were performed using a Carl Zeiss Merlin SEM at working distances between 5 and 10 mm, 2 nA probe current and 5 kV accelerating voltage for better spatial resolution and noise reduction. A windowless detector was chosen such that Li

Table 1
Composition of Eurofer97 in wt% [17].

Fe	Cr	Mn	V	Ta	W	C	N	Ni	Nb	Mo
Bal.	8.95	0.55	0.20	0.14	1.04	0.11	0.038	0.03	0.004	0.005

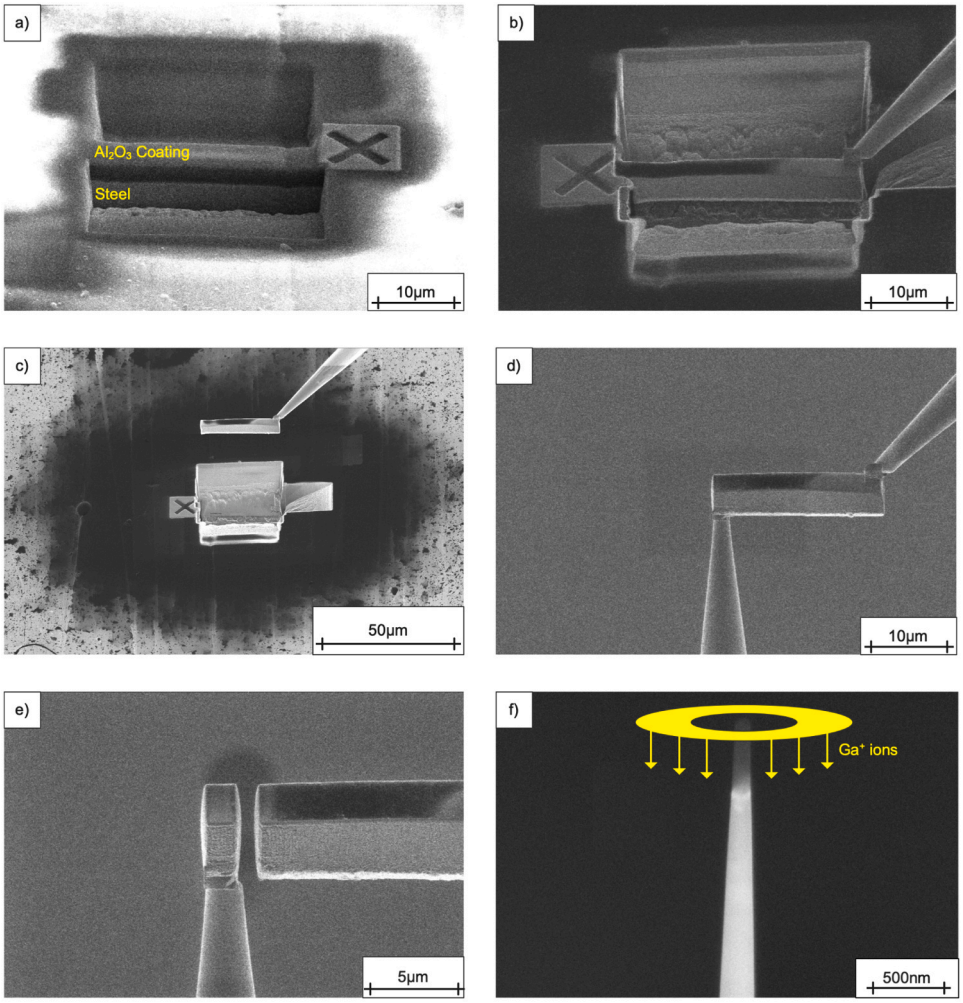

Fig. 2. FIB-based APT sample preparation. a)trenching; b)undercutting; c)lift-out; d)attachment to Si micro-tip e)isolation from bulk; f)annular milling.

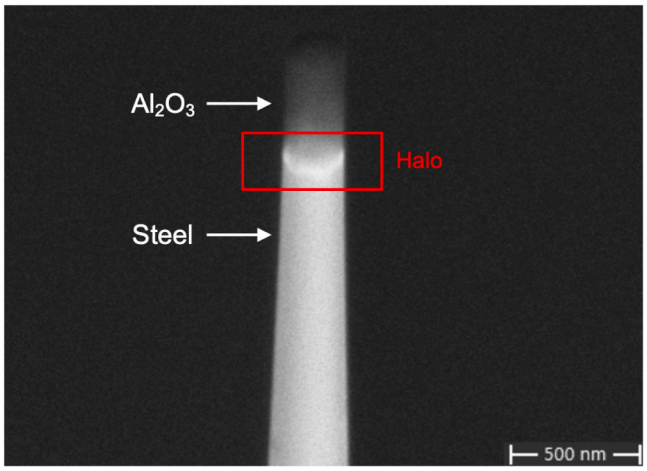

Fig. 3. SEM-BSE image of an intermediate stage in the preparation for an APT sample.

atoms could be potentially detected. The results were analysed with Oxford Instrument's AZtec software.

3. Results and discussion

3.1. Microscale characterization

Prior to the experiments, it was hypothesized that most of the inward-diffusing lithium was trapped within the Al_2O_3 coating. A SEM-backscattered electron (BSE) image and the accompanying EDX maps of the coating are presented in Fig. 4. There exists a faint contrast that is more prominent near the central region of the coating. The contrast likely originated from density variations within the coating, where darker regions may have undergone a change in crystallinity. This implies the coating is no longer fully amorphous after prolonged exposure to Pb-17Li at temperature.

The composition of the coating determined using EDX is 40 at% Al and 51 at% O, close to the theoretical O/Al ratio of 1.5 with the main impurity being 9 at% C. The deviation of O from 60 at% is likely a result of EDX underestimating light elements. Taking this into consideration, the results demonstrate PLD was able to produce a coating close to the target composition of Al_2O_3. The absence of any interfacial delamination or large through-thickness cracks in the image also showed that the coating remained macroscopically intact after 7000 h exposure to Pb-17Li.

No Li was detected by EDX and it is speculated that the concentration of Li in the X-ray interaction volume is probably too low for it to be

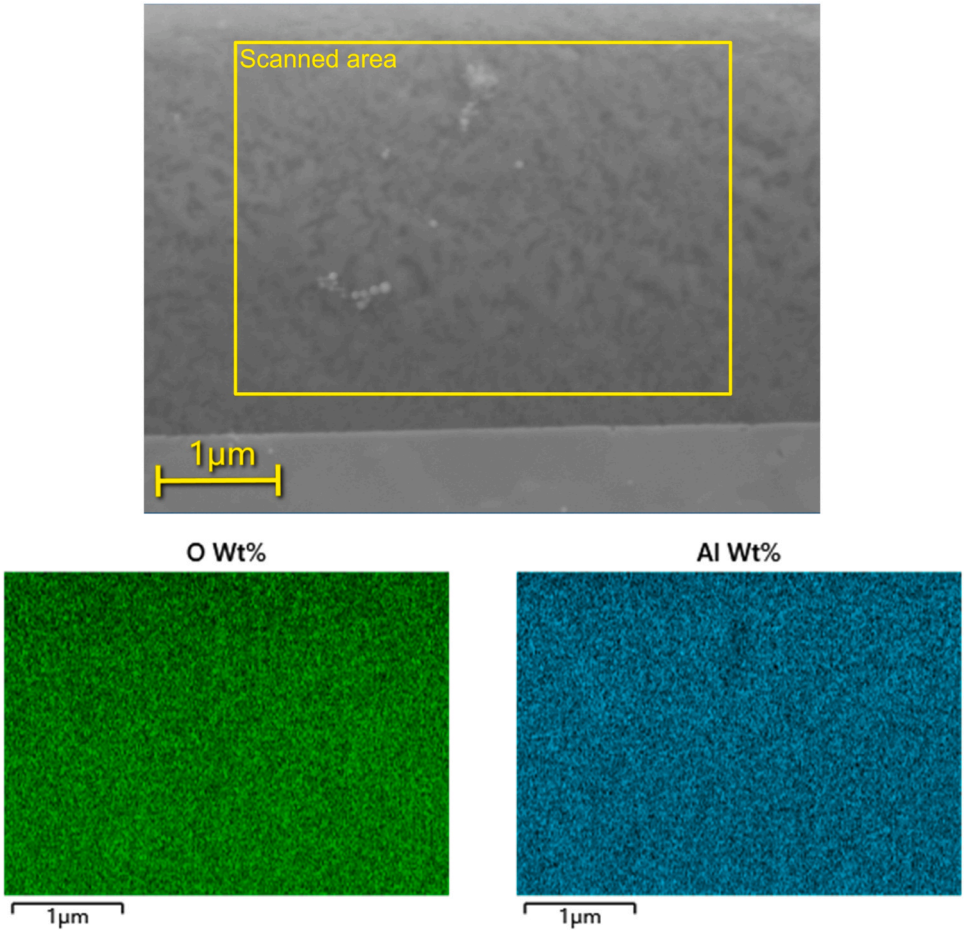

Fig. 4. SEM-BSE image and EDX element maps of PLD-Al_2O_3 coating after immersion for 7000 h.

detected. Works on Y_2O_3 and Er_2O_3 barrier coatings [12,14] make it certain that Li is able to diffuse through ceramics, and its absence here is attributed to limited chemical sensitivity of the instrument. The incorporation of Li into PLD-Al_2O_3 has been documented using SIMS previously [6], however, the authors did not report a quantitative concentration allowing for direct comparison.

3.2. APT characterization of Al_2O_3 coating

Despite the difficulty in locating the precise ceramic-steel interface using SEM/FIB, multiple APT specimens were extracted from the regions approximately within 50 nm from the interface. The average composition of each specimen was extracted and is displayed in Fig. 5. Ceramic samples tend to field evaporate with a high ratio of complex ions, and these are decomposed by the APT analysis software into their constituent atomic species. The dotted horizontal lines in Fig. 5. mark the theoretical compositions of Al and O. A deviation of Al and O from stoichiometry is accompanied by a non-zero amount of Li detected in all samples. This means corrosion attack, in some cases significant, has occurred.

Contrary to the claim by Gasquez et al.[6] that the Pb-17Li composition remains eutectic as it moves through the coating, all four samples only contained Li, Al and O atoms. Although the random atomic arrangement makes diffusion pathways less certain, it is believed that Pb diffusion remains difficult in amorphous Al_2O_3 due to its much larger radius than both Al and O. The detection of Pb near the ceramic-steel interface, as indicated by the author themselves, is more likely a result of the liquid breeder penetrating through defects than by diffusion. Our results are in line with those obtained by Petras et al.[11] where the ingression of Pb atom is completely stopped by the coating.

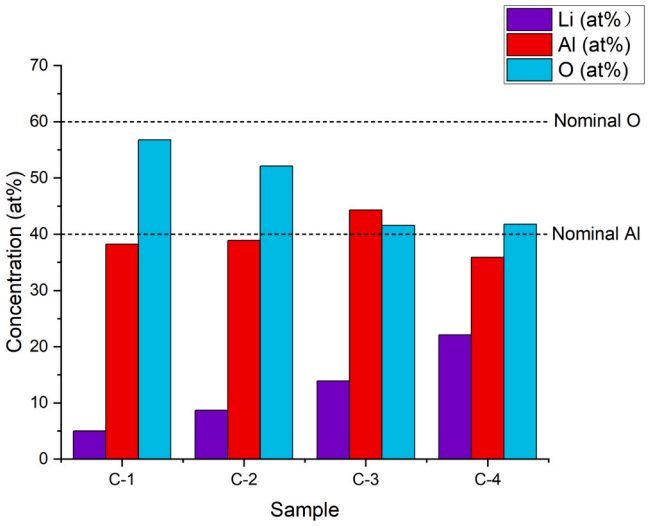

Fig. 5. Average composition of the analysed volume in four APT measurements of the coatings (C1-C4).

The systematic loss of O signals in APT studies of oxides have been attributed to be an artefact from data collection. One explanation is through multiple-hit events, which occur when multiple ions are simultaneously evaporated by one pulse [19]. The detector is then unable to spatially resolve the two if they arrive close in time and location.

It is also accepted that the dissociation of complex ions en-route to the detector may result in the generation of neutral oxygen molecules that are unaffected by the electric field and lost to the analysis [20] For example, Liu et al.[21] measured a sub-stoichiometric oxygen concentration (54 at%) in thermally grown Al_2O_3 on steel substrates. Although this O loss needs to be treated with caution when describing the measured composition, it is impossible to isolate the contribution from experimental artefacts to the observed O deficit at this stage. While correlative histograms may help relate the systematic O loss to specific field dissociation events, they are unable to quantitatively evaluate the extent of the problem. Additionally, the use of a reflectron in this setup prevents their implementation [22].

Sample 1 and 2 indicate it is possible to obtain near-stoichiometric matrix composition with current experimental parameters. Previous APT analyses on as-fabricated PLD nano-alumina returned a similar composition of 42at%Al and 56at%O [23]. Furthermore, O deficit reported for Fe and Cr based oxides with known reference compositions typically range between 3 at% and 6 at% [24,25]. Hence, it is unlikely that artefacts are solely responsible for the observed deficit of over 15 at % O in samples 3 and 4. The change in Li:A:O ratio between samples may instead point towards lithium inhomogeneity on the scale of the volumes sampled by atom probe and the existence of Li-induced microstructural changes.

3D reconstruction for each APT sample with respective iso-concentration surfaces highlighting Li enrichment therein are presented in Fig. 6. The iso-concentration surfaces delineate regions within the data with a user-defined Li concentration, such that the region enclosed has a higher Li content and vice versa. A voxel size of 1 nm^3 was used for all iso-surfaces with delocalization distances in the x, y and z directions being 3 nm, 3 nm and 1.5 nm respectively. For visual clarity, complex ions are not displayed while the matrix atoms are presented in similar colours. The presence of Li-enriched microstructural features, is clearly evident. The iso-concentration values were chosen to be the average Li concentration between the matrix containing no Li-enriched features and the centre of the largest Li-enriched feature respectively.

In C-1 the observed Li-enriched features are discrete and relatively smaller compared to C-2 and C-4 where larger, continuous features percolates through the matrix. In the case of C-4, the feature expands beyond the atom probe field of view, such that only the top and bottom surfaces could be defined. The Li iso-concentration values of larger features can approach 20 at% and they are significantly more enriched than smaller ones. The different size and composition of the Li-enriched features explains the variation in the overall sample composition reported in Fig. 5.

3.3. Origin of Li-enriched features

Li has been previously observed in solid solution in the near-surface region of amorphous Al_2O_3 immersed in liquid Pb-17Li for 4000 h [23], hence raising questions on the origin of the Li-enriched features. It is necessary to ensure that the observed microstructure is not an effect of

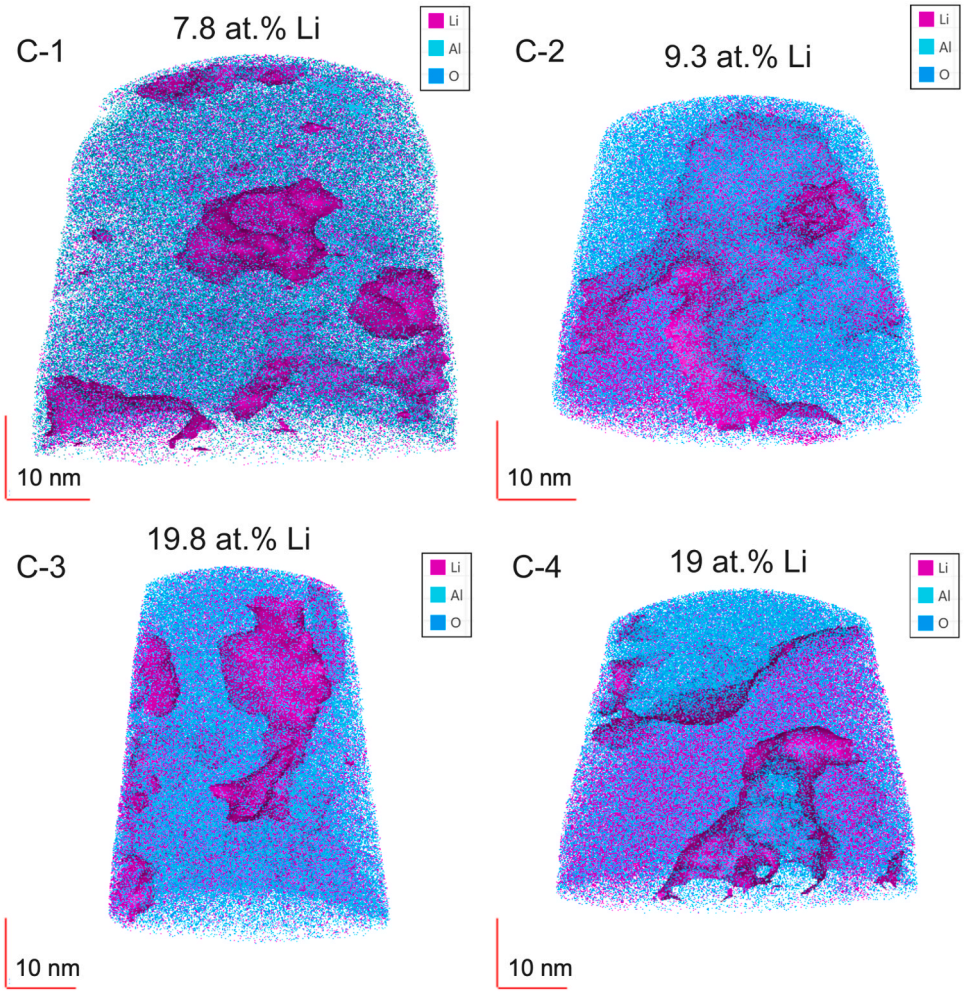

Fig. 6. APT reconstructions of Pb-17Li exposed Al_2O_3 specimens, iso-concentration surfaces highlight regions of enriched Li. The iso-concentration value chosen for each sample is displayed above the corresponding reconstruction.

the highly mobile Li ions migrating during the analysis under the influence of the very high electric field applied in the APT experiment. *In situ* Li migration was demonstrated during APT experiments of Li-containing ceramics [26], leading to erroneous characterization of the Li distribution prior to the analysis. The study also showed that contrary to what might initially be assumed as best practice, the effect was actually suppressed by not transferring APT specimen under ultra-high vacuum (UHV) between the FIB and the atom probe instruments, respectively. Researchers found that accurate analysis could be achieved where post-FIB specimen were simply transferred through air, under ambient temperature and pressure into the atom probe. During transfer, a thin conductive oxide layer described in [26] was likely able to form on the Al_2O_3 surface to provide intrinsic shielding from the electric field that otherwise would have caused movement of Li atoms. One possible mechanism for this surface modification is through adsorption of moisture at room temperature, which was previously shown to increase the conductance of Al_2O_3[27].

Fig. 7 shows the 1-D concentration profile through a cylindrical ROI in sample C-3, the sample containing Li-enriched features with the highest Li content. If the migration mechanism was in effect, we would expect a much higher concentration of Li atoms near the top part of the reconstruction, corresponding to the apex of the specimen, where the highest electric field is generated. Instead, the Li concentration profile remains relatively flat across and is lower than those found within the features. It would indicate the Li-enriched features are forming in regions away from the specimen tip, and their high Li concentrations are thus not the effect of *in situ* delithiation. This supports our theory that the observed Li-enriched features are corrosion products and not a field-induced artefact.

3.4. Analysis of corrosion products

Fig. 8 shows the transition of Al, O and Li concentrations across the matrix-feature interface as a function of distance perpendicular to a user defined iso-concentration surface. The thresholds used to define relative positions of the interface were selected in the same manner as those in Fig. 6, where the average Li concentration between the matrix and the centre of the largest feature in each sample was taken. Data presented here only includes the largest Li-enriched feature in each experiment.

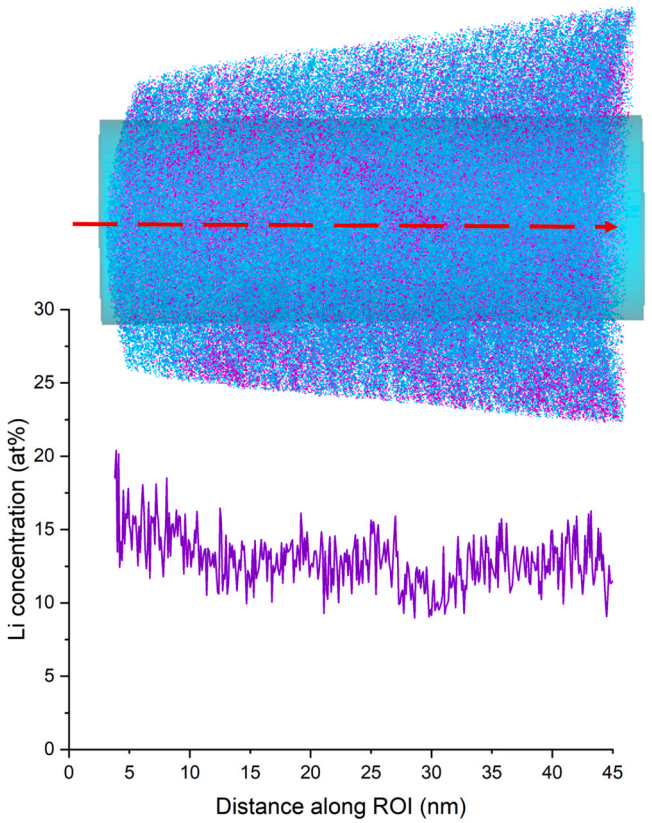

Fig. 7. 1-D Li concentration profile of C-3 along the indicated cylindrical ROI.

According to Fig. 8, a maximum of 10 at% Li can be detected in the Al_2O_3 matrix. This is almost identical to the Li concentration observed near the surface by DiFonzo [23] in a similar sample exposed to Pb-17Li at 550°C for 4000 h, where one expects the highest Li content. Together, they indicate the solubility limit of Li in Al_2O_3 at 550°C might be around 10 at%. The exact reason why C-1 and C-2 contained Li-enriched features with a matrix Li content of only 5 at% is unclear. However, it is believed that local variations in the Li concentration and the limited field of view of APT both contribute to this observation. The Li concentration increases inside the interface, accompanied by a drop in Al, while the O behaviour varies. It is apparent that the features exhibit two distinct concentration changes across the interface. In the small feature found in C-1, the matrix O content is roughly stoichiometric and consistent across the interface. The increase of Li from less than 5 at% in the matrix to 12 at% in the feature is quite shallow over a distance of 4 nm. The Al content is also around 5 at% lower than stoichiometry and further decreases in the Li-enriched features. Therefore, it is assumed that Li replaces some Al in the structure during early stages of corrosion. Trends in C-2 are very similar except that O drops slightly within the features and the Li content increases to 15 at%.

For C-3 and C-4, the adjacent matrix has a significantly lower O content which decreases to ~40 at% in the Li-enriched features. Even though the Al concentration is roughly stoichiometric in the Al_2O_3 matrix, it decreases to around 30 at% within the features, which is similar to the observed Li concentration. The interface, across which the Li content triples, is narrower and more pronounced. A proxigram analysis was created for both top and bottom surfaces of the biggest feature in C-4 and yielded the same profile. This leads to the assumption that the Li-rich features observed in the two sample are at the same stage of the corrosion process. The depletion of O could be a combination of the aforementioned experimental artefacts and long-range diffusive interactions during later stages of corrosion.

The pre-defined iso-concentration surface marks the zero point on proxigrams x-axis [28], but here the actual interface is slightly shifted. In this case, the interface was difficult to define and measure the Li concentration within them is affected their size and shape. A list of average Li:Al:O ratios inside several selected Li-enriched features has been enumerated alongside their respective volume in Table 2.

The absolute lengths and shape of the microstructural features cannot be definitively determined because the commonly used calibration method for APT datasets does not apply to amorphous oxides. Their volumes, however, is independent of reconstruction parameters and thus chosen as a variable to correlate with Li-content of the features. While this is true, the largest Li-enriched features in the datasets appear truncated and not fully captured by the analysed volumes. This is emphasised by the "$>$" sign in Table 2 and the values should be considered a lower limit of the selected feature.

The obtained Li:Al:O ratios do not correspond to any equilibrium ternary compounds on the Li_2O-Al_2O_3 phase diagram [29]. They also fall below those for the most stable amorphous lithiated alumina at 300 K ($Li_{3.4}Al_2O_3$) predicted by *ab initio* molecular dynamics [30]. The very diffuse interface between the Li-enriched features and the matrix makes it difficult to rationalize the non-equilibrium ratios, namely 1:0.9:1.2 and from 1:2.5:3.6–1:2.5:5.0. Nevertheless, it is highly improbable that the features remain metastable after spending 7000 h at 823 K.

During the annular milling stage of the FIB lift-out process, it was very challenging to measure the position of the APT tips relative to the surface in contact with Pb-17Li. There was no reliable method to track the rate of material removal by the ion beam and the samples could only be quoted as within 50 nm from the ceramic-metal interface. This

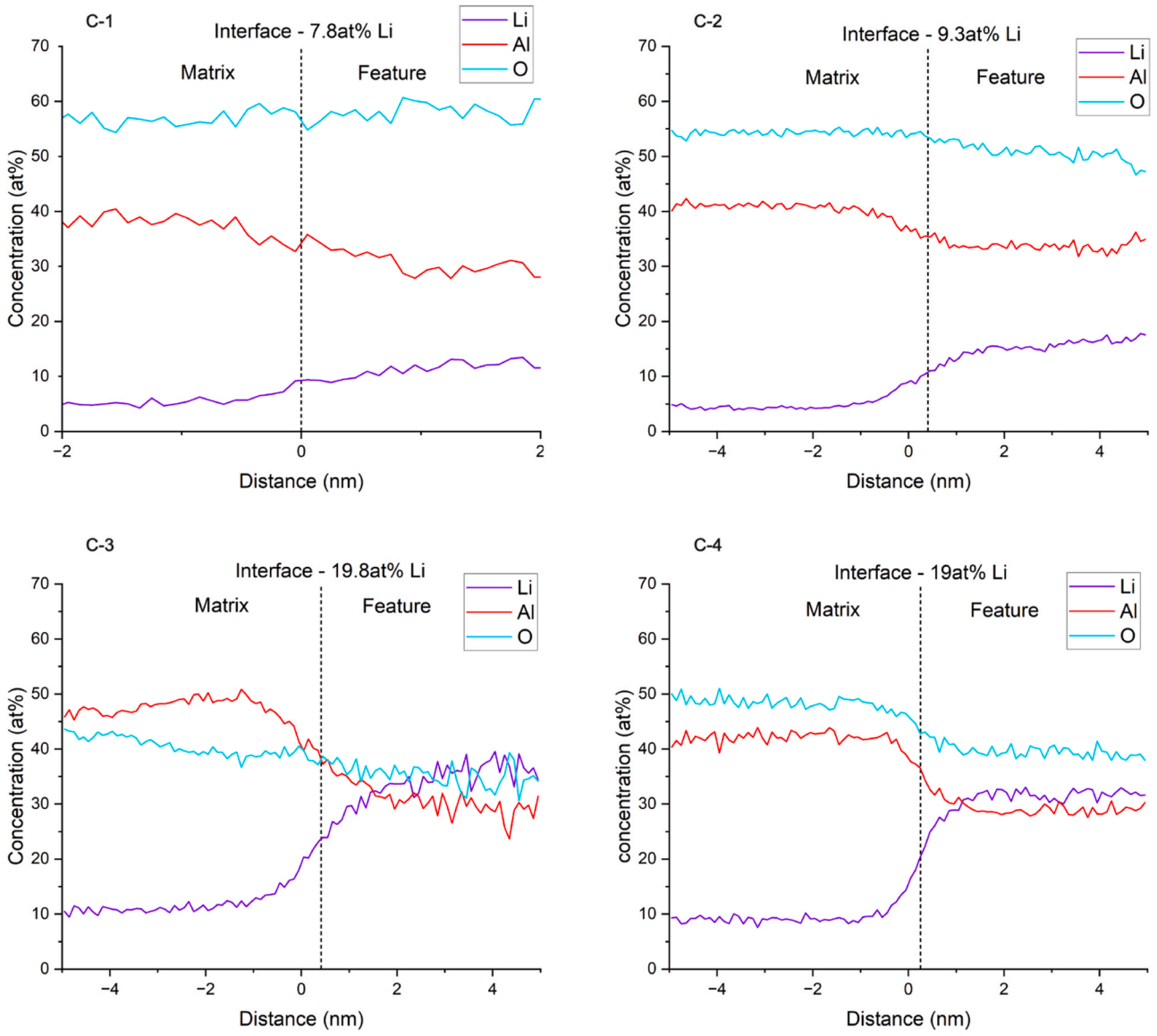

Fig. 8. Proximity histogram analysis of the largest Li-enriched feature within specimens C-1 to C-4.

Table 2
Li:Al:O ratios and volumes for selected features.

Specimen	Li:Al:O	Volume (nm^3)
C−1	1:2.5:5.0	>1000
	1:2.8:4.9	>990
	1:2.8:4.9	>440
	1:2.9:5.0	>280
C−2	1:2.0:3.0	>12000
	1:2.5:3.6	>740
C−3	1:1.0:1.1	>3400
	1:1.0:1.2	>1300
C−4	1:0.9:1.2	>30000

uncertainty in the final tip location would mean that the APT samples containing a higher Li concentration may have been extracted from a region where the corrosion process had taken place longer. Based on the observation that the Li-enriched features with a Li:A:O ratio of 1:0.9:1.2 do not appear in samples C-1 and C-2, it is believed the two feature types represent different stages of corrosion. The change in composition with size is not significant for highly Li- enriched features, meaning the outward growth of these features may dominate over further Li ingression at the later stages of corrosion.

3.5. *Composition evolution in the Al_2O_3 coating*

Compositions of the matrix and Li-enriched features have been plotted in a Li-Al-O ternary diagram in Fig. 9. for better visualization. Known compounds predicted to be stable by Zhu et al.[31] have also been included.

Matrix compositions (purple dots) are centred around a region between pristine Al_2O_3 and the spinel $LiAl_5O_8$, despite the slight differences in O. Li is likely in solid solution in the matrix and unable to undergo phase changes. The Li-enriched features (red squares), on the other hand, appear to be divided into two regions: one between Al_2O_3 and $LiAlO_2$ and the other between $LiAlO_2$ and LiAl.

Interestingly, the features with lower Li found in C-1 fall close to the vertical section of the Gibbs triangle corresponding to the Al_2O_3 and Li_2O binary phase diagram shown in Fig. 10. It was initially assumed that these features comprise a mixture of $LiAlO_2$ and $LiAl_5O_8$, because the Li:Al:O ratio of 1:2.8:4.9, if approximated as 1:3:5, can be partitioned into $LiO_{0.5}$+$3AlO_{1.5}$ which is indicated by the red line in Fig. 10. The first stage of corrosion may therefore be the formation of a $LiAl_5O_8$-

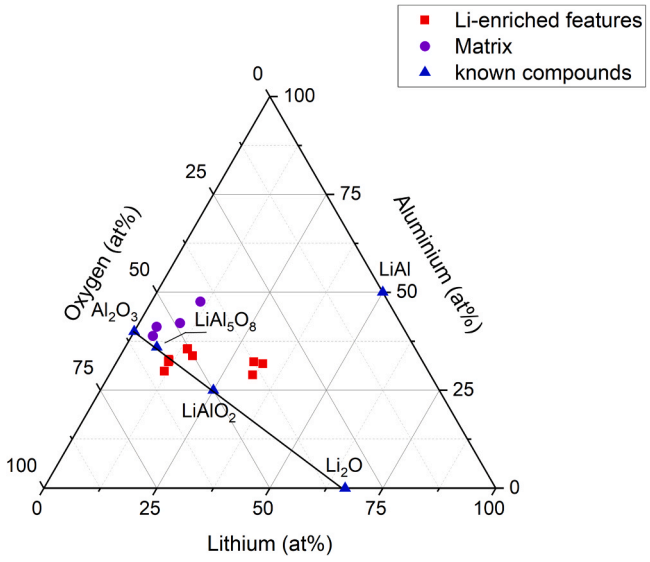

Fig. 9. Li-Al-O ternary diagram indicating measured compositions of the matrix and the Li-enriched features.

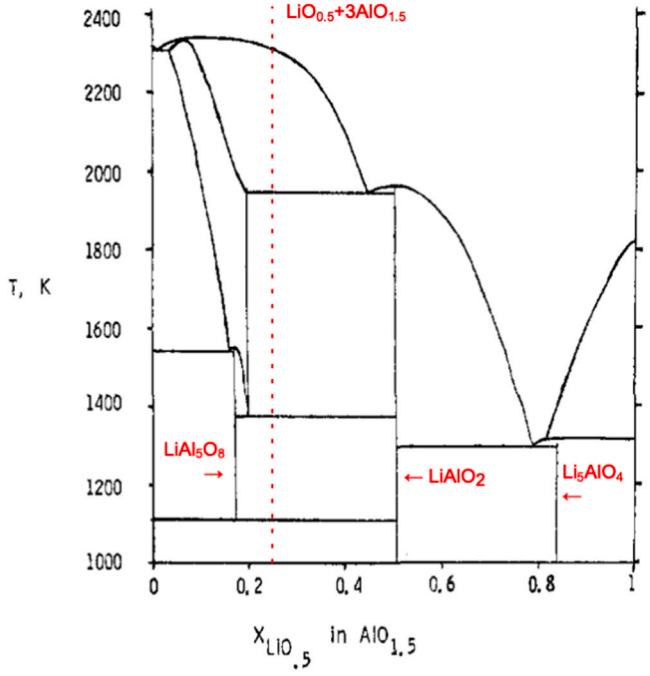

Fig. 10. Li_2O-Al_2O_3 binary phase diagram adapted with permission from[32], Copyright 1979 American Chemical Society. The red line marks the compound with Li:Al:O of 1:3:5.

$LiAlO_2$ dual phase. However, further analysis using respective Li iso-concentration surfaces at 7.14 at% ($LiAl_5O_8$) and 25 at% ($LiAlO_2$) reveals that the $LiAlO_2$ composition is never reached even at the core of the features, where the Li concentration is the highest. The Li-enriched features are therefore unlikely a mixture of equilibrium phases.

The larger Li-enriched features found in C-3 and C-4 with a high Li content reinforces this speculation, as they cannot be partitioned into a combination of two equilibrium phases. In the ternary phase diagram, Fig. 9, they are separated from the smaller ones by a significant increase in Li which points towards a further lithiation step similar to those seen in battery charging. The same iso-concentration thresholds of 7.14 at% Li and 25 at% Li highlights a completely different region of space, as seen in Fig. 11. The polygons with a 7.14 at% iso-surface appear discrete, while increasing the Li concentration value further to 25 at% Li highlights a different region in the reconstruction where the features are now larger and continuous. The fact that the two types of Li-enriched features do not overlap spatially in C-3 reinforces the speculation of there being two stages of corrosion. The features defined by the 25 at% iso-surface are smaller in size but similar in shape to those defined by the 19.8 at% Li surface found in Fig. 6. for the same reconstruction. It signifies the concentration of Li gradually increases towards the feature core before it peaks, such that they cannot be a homogenous phase with a well-defined composition. Hence, it is believed that the Li-enriched features are regions of unevenly lithiated Al_2O_3.

The lithiation of α-Al_2O_3 at 873 K after 250 h was determined by Kondo et al.[33] to follow Eqs. (1) and (2):

$$\alpha\text{-}Al_2O_3 + 2Li_{(LiPb)} + O_{(LiPb)} \rightarrow 2\alpha/\gamma\text{-}LiAlO_2 \quad (1)$$

$$\alpha\text{-}Al_2O_3 + 1.5Li_{(LiPb)} + O_{(LiPb)} \rightarrow 1.5\alpha/\gamma\text{-}LiAlO_2 + 0.5Al \quad (2)$$

This mechanism does not apply to amorphous Al_2O_3 as experimental evidence presented in this work suggest. Observation accompanying the above process, including the formation and growth of a $LiAlO_2$ surface layer, was absent in the SEM cross sectional image (Fig. 1). Results by DiFonzo [23] further show that Li forms a 10 at% solid solution within the first 10 nm of the amorphous Al_2O_3 exposed to Pb17Li at 823 K for 4000 h. It is therefore evident that amorphous Al_2O_3 undergoes an alternative lithiation process compared to its crystalline counterpart. A possible mechanism is proposed as follows:

The lithiation process would involve Li substitution of Al, shifting the composition from pristine Al_2O_3 to the Li-rich corner in Fig. 9. The lithiation is so severe that the core of the Li- enriched features can attain a composition approaching LiAlO. This can be rationalized by considering the following mechanisms:

1. The lithiation process forms one O vacancy from every Li substitution event. And contributes to the loss of O.
2. Part of the charge imbalance is compensated by the reduction of Al^{3+} to Al^{+} during lithiation [30], such that $Li^{+}Al^{+}O^{2-}$ is locally stable and charge neutral.

However, it is difficult to conclude from current findings if O is physically transported elsewhere or it is removed by the large influx of Li creating sufficient vacancies. The lack of a crystalline structure means that conventional phase identification techniques, e.g. X-ray diffraction, are unable to help track microstructural variations on length scales much larger than the analysis volume of APT.

Replacement of Al with Li should stop at the composition of $Li_2Al_2O_3$ as beyond this the structure would be electrostatically unstable [30]. This corresponds to a Li:Al:O ratio of 1:1:1.5, which is close to the 1:1:1.2 ratio found in the larger Li-enriched features, proving that the experimental results are in agreement with this computational prediction.

Previous studies [30,33] suggested that the lithiation is only complete when the whole Al_2O_3 reaches the thermodynamic stable phase. The concentration gradient within the features would indicate an incomplete corrosion process at 7000 h and formation of the theoretically most stable $Li_{3.4}Al_2O_3$ phase, if possible, requires longer immersion times in Pb-17Li.

Regardless, the formation of Li-rich phases is detrimental to the performance of the component in service. Not only does transmutation of Li to He near the interface pose a risk of coating delamination from cavities, but the diffusivity of Li is also more rapid in lithiated Al_2O_3[30], meaning the corrosion process is considered autocatalytic.

4. Conclusions

In this research, atom probe tomography was used to characterize

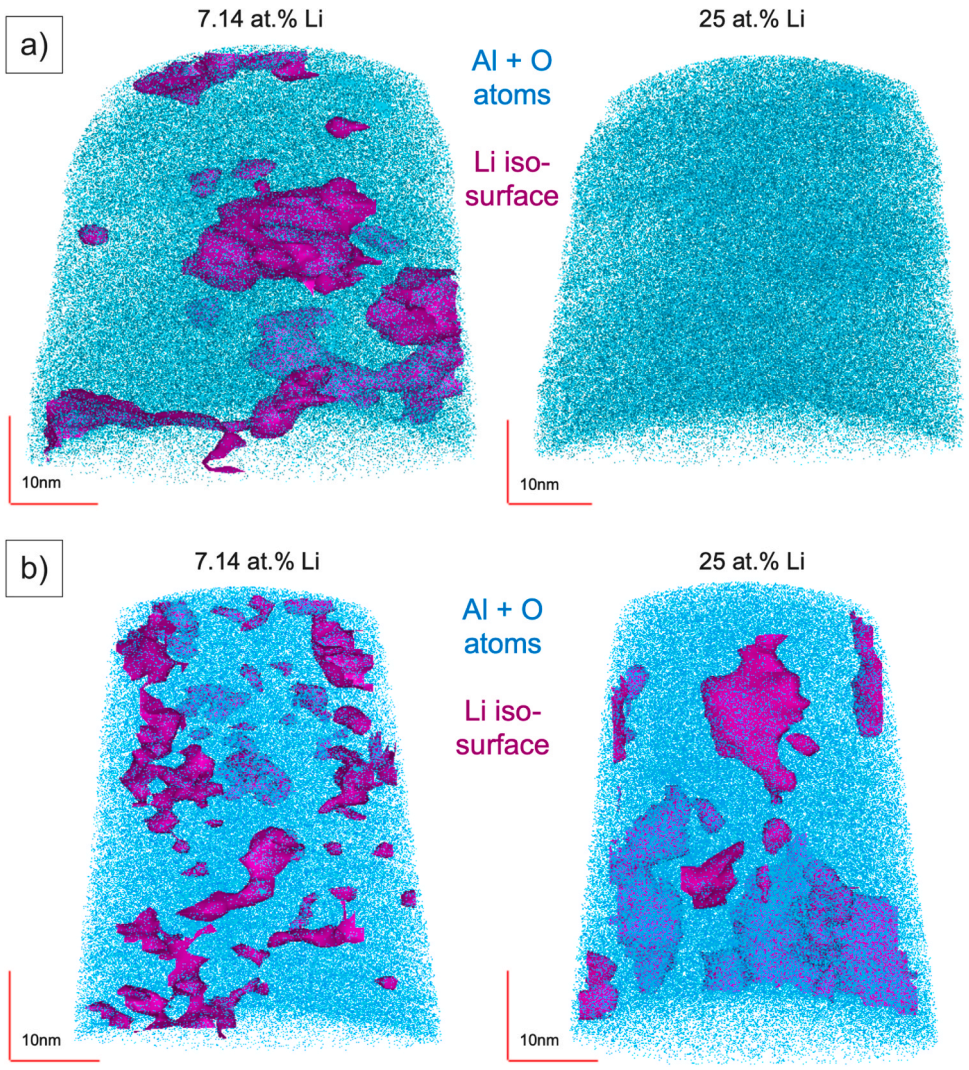

Fig. 11. Iso-concentration surfaces at 7.14 at% Li and 25 at% Li for a) C-1 and b) C-3.

the atomic scale changes in an Al_2O_3 barrier coating for Eurofer97 steel caused by lithium penetration, after exposure to Pb-17Li for 7000 h at 823 K. The findings are summarized as follows:

- Pulsed Laser Deposited Al_2O_3 is susceptible to Pb-17Li corrosion. While the coating acts as a diffusion barrier to Pb atoms, Li was found to be non-homogeneously distributed near the ceramic-steel interface
- Two types of Li- enriched features were observed, which seem to correspond to two products inherent to different stages of the corrosion process
- The Li- enriched features are lithiated Al_2O_3 instead of a mixture of equilibrium phases predicted by the phase diagram. The concentration of Li is highest in the core of the Li- enriched features, and gradually decreases towards the edges.
- The corrosion mechanism is suggested to be mainly via lithiation through Li substitution of Al with O removal and reduction of Al^{3+} to compensate for the charge imbalance.

CRediT authorship contribution statement

Christina Hofer: Writing – review & editing, Supervision, Resources, Project administration. **Michael P. Moody:** Writing – review & editing, Validation, Supervision, Conceptualization. **Andrew J. London:** Writing – review & editing, Validation, Supervision, Methodology, Investigation, Conceptualization. **Andrew Bulla:** Writing – review & editing, Writing – original draft, Validation, Investigation, Formal analysis. **Paul A.J. Bagot:** Writing – review & editing, Validation, Supervision, Resources, Conceptualization.

Declaration of Competing Interest

The authors declare that they have no known competing financial interests or personal relationships that could have appeared to influence the work reported in this paper.

Data availability

Data will be made available on request.

Acknowledgement

This research used UKAEA's Materials Research Facility, which has been funded by and is part of the UK's National Nuclear User Facility and Henry Royce Institute for Advanced Materials. The atom probe facilities at the University of Oxford are funded by the EPSRC grant EP/T011505/1. The authors would like to express their gratitude to Fabio Di Fonzo from the Italian Institute of Technology for kindly preparing the coated samples, and to Marco Utili (ENEA) for exposing the samples to Pb-Li. This work has been carried out within the framework of the

EUROfusion Consortium, funded by the European Union via the Euratom Research and Training Programme (Grant Agreement No 101052200 — EUROfusion) and from the EPSRC [grant number EP/W006839/1]. Views and opinions expressed are however those of the author(s) only and do not necessarily reflect those of the European Union or the European Commission. Neither the European Union nor the European Commission can be held responsible for them.

References

[1] M. Utili, et al., Status of Pb-16Li technologies for European DEMO fusion reactor, Fusion Eng. Des. vol. 146 (2019) 2676–2681.
[2] S. Malang, R. Mattas, Comparison of lithium and the eutectic lead-lithium alloy, two candidate liquid metal breeder materials for self-cooled blankets, Fusion Eng. Des. vol. 27 (1995) 399–406.
[3] S. Bassini, V. Cuzzola, A. Antonelli, M. Utili, Long-term corrosion behavior of EUROFER RAFM steel in static liquid Pb-16Li at 550C, Fusion Eng. Des. vol. 160 (2020) 111829.
[4] H. Glasbrenner, J. Konys, Z. Voß, Corrosion behaviour of low activation steels in flowing Pb–17Li, J. Nucl. Mater. vol. 281 (2-3) (2000) 225–230.
[5] H. Glasbrenner, J. Konys, H. Röhrig, K. Stein-Fechner, Z. Voss, Corrosion of ferritic–martensitic steels in the eutectic Pb–17Li, J. Nucl. Mater. vol. 283 (2000) 1332–1335.
[6] M.C. Gazquez, S. Bassini, T. Hernandez, M. Utili, Al2O3 coating as barrier against corrosion in Pb-17Li, Fusion Eng. Des. vol. 124 (2017) 837–840.
[7] B. Van der Schaaf, et al., The development of EUROFER reduced activation steel, Fusion Eng. Des. vol. 69 (1-4) (2003) 197–203.
[8] F.G. Ferré, M. Ormellese, F. Di Fonzo, M. Beghi, Advanced Al2O3 coatings for high temperature operation of steels in heavy liquid metals: a preliminary study, Corros. Sci. vol. 77 (2013) 375–378.
[9] D. Smith, et al., Progress in coating development for fusion systems, Fusion Eng. Des. vol. 61 (2002) 629–641.
[10] F.G. Ferré, et al., The mechanical properties of a nanocrystalline Al2O3/a-Al2O3 composite coating measured by nanoindentation and Brillouin spectroscopy, Acta Mater. vol. 61 (7) (2013) 2662–2670.
[11] R. Petráš, et al., Characterization of aluminum-based coatings after short term exposure during irradiation campaign in the LVR-15 fission reactor, Fusion Eng. Des. vol. 170 (2021) 112521.
[12] T. Terai, et al., Compatibility of yttria (Y2O3) with liquid lithium, J. Nucl. Mater. vol. 233 (1996) 1421–1426.
[13] M. Nagura, A. Suzuki, T. Terai, Corrosion prevention of Er2O3 by O control in Li, J. Nucl. Mater. vol. 417 (1-3) (2011) 1210–1213.
[14] Y. Li, C. Ke, X. Liu, F. Gou, X. Duan, Y. Zhao, Analysis liquid lithium corrosion resistance of Er2O3 coating revealed by LIBS technique, Fusion Eng. Des. vol. 136 (2018) 1640–1646.
[15] X. Chen, et al., Mechanical properties and microstructure characterization of Eurofer97 steel variants in EUROfusion program, Fusion Eng. Des. vol. 146 (2019) 2227–2232.
[16] D. Iadicicco, et al., Multifunctional nanoceramic coatings for future generation nuclear systems, Fusion Eng. Des. vol. 146 (2019) 1628–1632.
[17] L. Tan, et al., Recent status and improvement of reduced-activation ferritic-martensitic steels for high-temperature service, J. Nucl. Mater. vol. 479 (2016) 515–523.
[18] K. Thompson, D. Lawrence, D. Larson, J. Olson, T. Kelly, B. Gorman, In situ site-specific specimen preparation for atom probe tomography, Ultramicroscopy vol. 107 (2-3) (2007) 131–139.
[19] B. Gault, M.P. Moody, J.M. Cairney, S.P. Ringer, Atom Probe Microscopy, Springer Science & Business Media, 2012.
[20] B. Gault, et al., Behavior of molecules and molecular ions near a field emitter, N. J. Phys. vol. 18 (3) (2016) 033031.
[21] F. Liu, M. Halvarsson, K. Hellström, J.-E. Svensson, L.-G. Johansson, First three-dimensional atomic resolution investigation of thermally grown oxide on a FeCrAl alloy, Oxid. Met. vol. 83 (5) (2015) 441–451.
[22] D. Saxey, Correlated ion analysis and the interpretation of atom probe mass spectra, Ultramicroscopy vol. 111 (6) (2011) 473–479.
[23] F. DiFonzo, Meeting EUROfusion, Italian Institute of Technology, February 2022, 2022.
[24] A. La Fontaine, H.-W. Yen, P.J. Felfer, S.P. Ringer, J.M. Cairney, Atom probe study of chromium oxide spinels formed during intergranular corrosion, Scr. Mater. vol. 99 (2015) 1–4.
[25] M. Bachhav, F. Danoix, B. Hannoyer, J.M. Bassat, R. Danoix, Investigation of O-18 enriched hematite (α-Fe2O3) by laser assisted atom probe tomography, Int. J. Mass Spectrom. vol. 335 (2013) 57–60.
[26] S.-H. Kim, et al., Atom probe analysis of electrode materials for Li-ion batteries: challenges and ways forward, J. Mater. Chem. A vol. 10 (9) (2022) 4926–4935.
[27] M. Caldararu, G. Postole, C. Hornoiu, V. Bratan, M. Dragan, N. Ionescu, Electrical conductivity of γ-Al2O3 at atmospheric pressure under dehydrating/hydrating conditions, Appl. Surf. Sci. vol. 181 (3-4) (2001) 255–264.
[28] O.C. Hellman, J.A. Vandenbroucke, J. Rüsing, D. Isheim, D.N. Seidman, Analysis of three-dimensional atom-probe data by the proximity histogram, Microsc. Microanal. vol. 6 (5) (2000) 437–444.
[29] A. Skokan, A. KfK-Euratom, Phase stability investigations in the ceramic breeder systems Li2O-Al2O3 and Li2O-ZrO2. Fusion Technology 1990, Elsevier, 1991, pp. 772–776.
[30] S.C. Jung, Y.-K. Han, How do Li atoms pass through the Al2O3 coating layer during lithiation in Li-ion batteries? J. Phys. Chem. Lett. vol. 4 (16) (2013) 2681–2685.
[31] Y. Zhu, X. He, Y. Mo, Strategies based on nitride materials chemistry to stabilize Li metal anode, Adv. Sci. vol. 4 (8) (2017) 1600517.
[32] H.J. Byker, I. Eliezer, N. Eliezer, R.A. Howald, Calculation of a phase diagram for the lithium oxide-aluminum oxide (LiO0.5-AlO1.5) system, 1979/09/01, J. Phys. Chem. vol. 83 (18) (1979) 2349–2355, https://doi.org/10.1021/j100481a009.
[33] M. Kondo, S. Hatakeyama, N. Oono, T. Nozawa, Corrosion-resistant materials for liquid LiPb fusion blanket in elevated temperature operation, Corros. Sci. vol. 197 (2022) 110070.